We are IntechOpen,
the world's leading publisher of
Open Access books
Built by scientists, for scientists

4,800
Open access books available

122,000
International authors and editors

135M
Downloads

Our authors are among the

154
Countries delivered to

TOP 1%
most cited scientists

12.2%
Contributors from top 500 universities

WEB OF SCIENCE™

Selection of our books indexed in the Book Citation Index
in Web of Science™ Core Collection (BKCI)

Interested in publishing with us?
Contact book.department@intechopen.com

Numbers displayed above are based on latest data collected.
For more information visit www.intechopen.com

Unusual Temperature Dependence of Zero-Field Ferromagnetic Resonance in Millimeter Wave Region on Al-Substituted ε-Fe$_2$O$_3$

Marie Yoshikiyo, Asuka Namai and Shin-ichi Ohkoshi

Additional information is available at the end of the chapter

1. Introduction

Insulating magnetic materials absorb electromagnetic waves. This absorption property is one of the important functions of magnetic materials, which is widely applied in our daily life as electromagnetic wave absorbers to avoid electromagnetic interference problems [1-5]. For example, spinel ferrites are used as absorbers for the present Wi-Fi communication, which uses 2.4 GHz and 5 GHz frequency waves. With the development of information technology, the demand is rising for sending heavy data such as high-resolution images at high speed. Recently, high-frequency electromagnetic waves in the frequency range of 30–300 GHz, called millimeter waves, are drawing attention as a promising carrier for the next generation wireless communication. For example, 76 GHz is an important frequency, which is beginning to be used for vehicle radars. There are also new audio products coming to use, applying millimeter wave communication in the 60 GHz region [6,7]. However, there had been no magnetic material that could absorb millimeter waves above 80 GHz before our report on ε-Fe$_2$O$_3$.

Well-known forms of Fe$_2$O$_3$ are α-Fe$_2$O$_3$ and γ-Fe$_2$O$_3$, commonly called as hematite and maghemite, respectively. However, our research group first succeeded in preparing a pure phase of ε-Fe$_2$O$_3$, which is a rare phase of iron oxide Fe$_2$O$_3$ that is scarcely found in nature [8–10]. Since then, its physical properties have been actively studied, and one of the representative properties is the gigantic coercive field (H_c) of 20 kilo-oersted (kOe) at room temperature [11–18]. We have also reported metal-substituted ε-Fe$_2$O$_3$ (ε-M_xFe$_{2–x}$O$_3$, M = In, Ga, Al, and Rh), and showed that this series absorb millimeter waves from 35–209 GHz at room temperature due to zero-field ferromagnetic resonance (so called natural resonance) [19-29]. ε-Fe$_2$O$_3$ based magnet is expected to be a leading absorbing material for the future wireless communication using higher frequency millimeter waves.

In this chapter, we first introduce the synthesis, crystal structure, magnetic properties, and the formation mechanism of the original ε-Fe$_2$O$_3$ [8–10]. Then we report the physical properties of Al-substituted ε-Fe$_2$O$_3$, mainly focusing on its millimeter wave absorption properties due to zero-field ferromagnetic resonance. The resonance frequency was widely controlled from 112–182 GHz by changing the aluminum substitution ratio [23]. Furthermore, from a scientific point of view, temperature dependence of zero-field ferromagnetic resonance was investigated and was found to show an anomalous behavior caused by the spin reorientation phenomenon [28].

2. ε-Fe$_2$O$_3$

This section introduces the synthesis, crystal structure, magnetic properties, and the formation mechanism of ε-Fe$_2$O$_3$. ε-Fe$_2$O$_3$ had only been known as impurity in iron oxide materials, and its properties were clarified for the first time after our success in the synthesis of single-phase ε-Fe$_2$O$_3$ in 2004 [8].

2.1. Synthesis, crystal structure, and magnetic properties of ε-Fe$_2$O$_3$

Single-phase ε-Fe$_2$O$_3$ nanoparticles are synthesized by a chemical method, combining reverse-micelle and sol-gel techniques (Figure 1) [8–10,16]. In the reverse-micelle step, two reverse-micelle systems, A and B, are formed by cetyl trimethyl ammonium bromide (CTAB) and 1-butanol in n-octane. Reverse-micelle A contains aqueous solution of Fe(NO$_3$)$_3$ and Ba(NO$_3$)$_2$, and reverse-micelle B contains NH$_3$ aqueous solution. These two microemulsion systems are mixed under rapid stirring. Tetraethoxysilane (C$_2$H$_5$O)$_4$Si is then added to this solution, which forms SiO$_2$ matrix around the Fe(OH)$_3$ nanoparticles through 20 hours of stirring. The precipitation is separated by centrifugation and sintered in air at 1000°C for 4 hours. The SiO$_2$ matrix is removed by stirring in NaOH solution at 60°C for 24 hours.
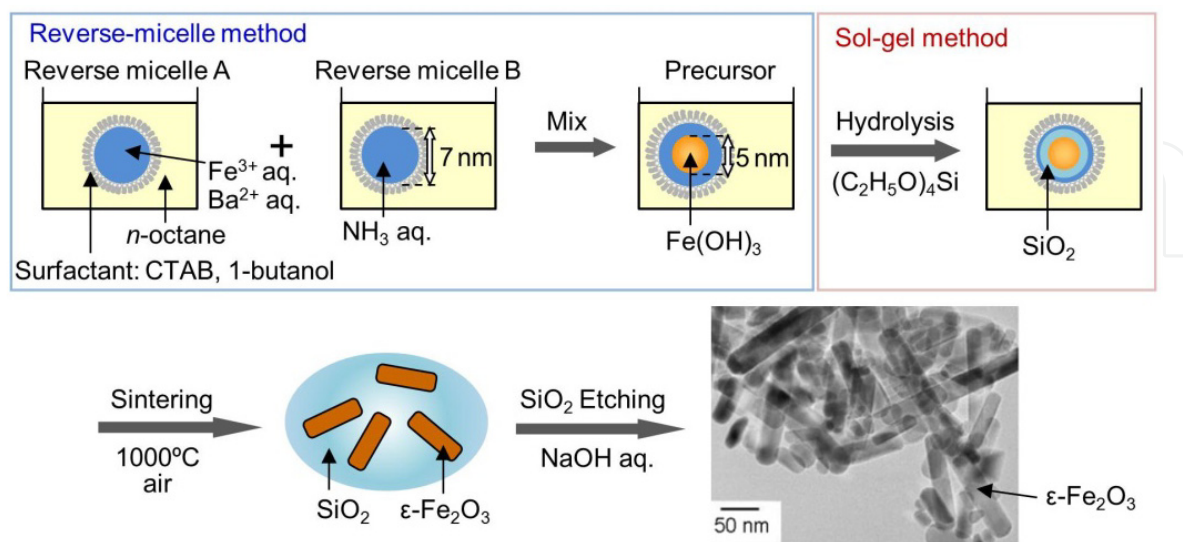

Figure 1. Synthetic procedure of ε-Fe$_2$O$_3$ nanomagnets using a combination method of reverse-micelle and sol-gel techniques. The inset is a transmission electron microscopy image of ε-Fe$_2$O$_3$ nanorods.

With this synthesis method, rod-shaped ε-Fe$_2$O$_3$ is obtained due to the effect of Ba^{2+} ions, which adsorb on particular planes of ε-Fe$_2$O$_3$, inducing growth towards one direction. Spherical ε-Fe$_2$O$_3$ nanoparticles can also be synthesized by a different method without Ba^{2+} ions, which is an impregnation method using mesoporous silica nanoparticles [17,29,30]. Methanol and water solution containing Fe(NO$_3$)$_3$ is immersed into mesoporous silica and heated in air at 1200°C for 4 hours. The etching process is the same as above.

The crystal structure of ε-Fe$_2$O$_3$ is shown in Figure 2a. It has an orthorhombic crystal structure (space group $Pna2_1$) with four non-equivalent Fe sites, A, B, C, and D sites. A, B, and C sites are six-coordinated octahedral sites, and D site is a four-coordinated tetrahedral site. ε-Fe$_2$O$_3$ exhibits spontaneous magnetization at a Curie temperature (T_C) of 500 K. Figure 2b presents magnetization versus external magnetic field curve at 300 K, which shows a huge H_c value of 20 kOe. Before this finding, the largest H_c value among metal oxide was 6 kOe of barium ferrite, BaFe$_{12}$O$_{19}$ [31], which indicates that the H_c of ε-Fe$_2$O$_3$ is over three times larger. The magnetic structure has been investigated using molecular field theory, which indicated that B and C sites have positive sublattice magnetizations, and A and D sites have negative sublattice magnetizations [32]. This result was consistent with the experimental results from neutron diffraction measurements, Mössbauer spectroscopy measurements, etc. [13,14], and was also consistent with first-principles calculation results [33].
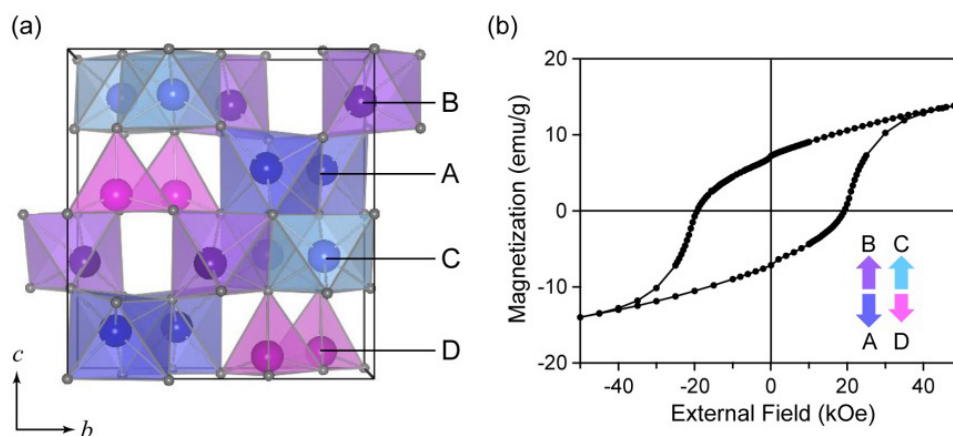

Figure 2. (a) Crystal structure of ε-Fe$_2$O$_3$. Dark blue, purple, light blue, and pink polyhedrons indicate A, B, C, and D sites, respectively. (b) Magnetization versus external magnetic field curve of ε-Fe$_2$O$_3$ at 300 K. Inset is a schematic illustration of the sublattice magnetizations of each site.

2.2. Formation mechanism of ε-Fe$_2$O$_3$

Here we discuss the formation mechanism of ε-Fe$_2$O$_3$ from the viewpoint of phase transformation. By changing the sintering temperature in the present synthesis, a phase transformation of γ-Fe$_2$O$_3$ $\rightarrow$ ε-Fe$_2$O$_3$ $\rightarrow$ α-Fe$_2$O$_3$ was observed accompanied by an increase of particle size. γ- and α-Fe$_2$O$_3$ are very common phases of Fe$_2$O$_3$, and it has been well known that γ-Fe$_2$O$_3$ transforms directly into α-Fe$_2$O$_3$ in a bulk form. In the present case, it is considered that ε-Fe$_2$O$_3$ appeared as a stable phase at an intermediate size region due to the

large surface energy effect. Free energy of each i-phase (G_i, $i = \gamma$, ε, or α) is expressed as a sum of chemical potential (μ_i) and surface energy ($A_i\sigma_i$):

$$G_i = \mu_i + A_i\sigma_i, \tag{1}$$

where A_i is molar surface area and σ_i is surface free energy of a particle. Since, A_i is equal to $6V_{m,i}/d$, where $V_{m,i}$ and d represent the molar volume and particle diameter, respectively, the free energy per molar volume is expressed as

$$G_i / V_{m,i} = \mu_i / V_{m,i} + 6\sigma_i / d. \tag{2}$$

This equation indicates that the contribution of the surface energy increases with the decrease of particle diameter. When the parameters satisfy the following three conditions, $\mu_\gamma > \mu_\varepsilon > \mu_\alpha$, $\sigma_\gamma < \sigma_\varepsilon < \sigma_\alpha$, and $(\sigma_\varepsilon - \sigma_\gamma)/(\sigma_\alpha - \sigma_\varepsilon) < (\mu_\varepsilon - \mu_\gamma)/(\mu_\alpha - \mu_\varepsilon)$, the free energy curve for each phase, $G_\gamma/V_{m,\gamma}$, $G_\varepsilon/V_{m,\varepsilon}$, and $G_\alpha/V_{m,\alpha}$ intersect to form ε-Fe_2O_3 as the most stable phase at an intermediate d value (Figure 3). Such nanosize effect has also been reported for other metal oxide materials, e.g. Al_2O_3 [34,35] and Ti_3O_5 [36].
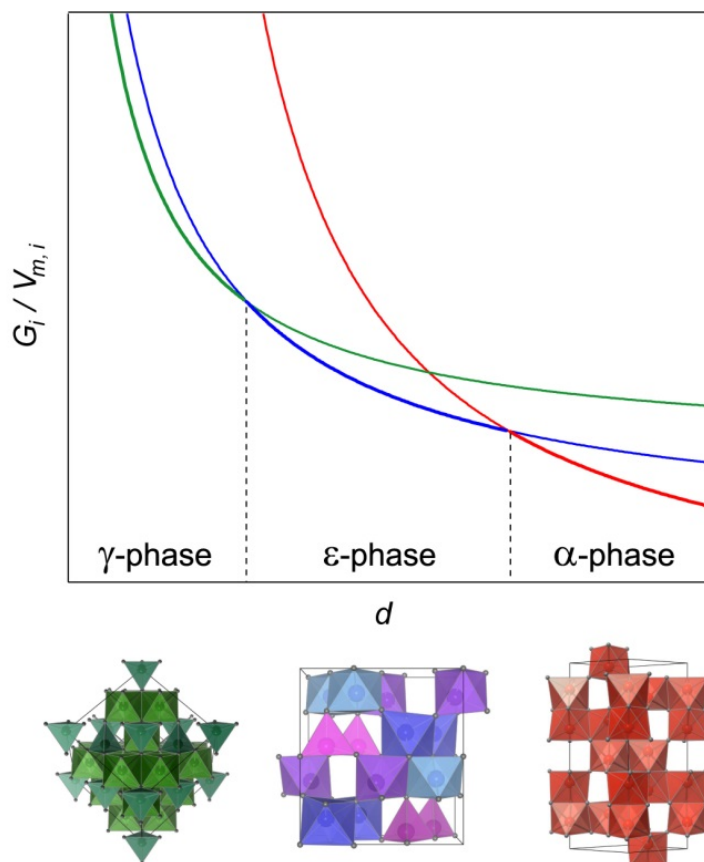

Figure 3. Representation of free energy per volume (G/V) versus particle diameter (d) for the three phases of Fe_2O_3. Green, blue, and red lines indicate the G/V curves for γ-Fe_2O_3, ε-Fe_2O_3, and α-Fe_2O_3, respectively. Below the graph are the crystal structures of γ-Fe_2O_3, ε-Fe_2O_3, and α-Fe_2O_3 from the left to right.

3. Al-substituted ε-Fe₂O₃

In this section, synthesis, crystal structure, and various physical properties of Al-substituted ε-Fe₂O₃, ε-Al$_x$Fe$_{2-x}$O₃, is discussed. Especially, the millimeter wave absorption property by zero-field ferromagnetic resonance is focused.

3.1. Synthesis of Al-substituted ε-Fe₂O₃

ε-Al$_x$Fe$_{2-x}$O₃ samples (x = 0.06, 0.09, 0.21, 0.30, 0.40) were synthesized by the same method as the original ε-Fe₂O₃, using the combination of reverse-micelle and sol-gel techniques. Reverse-micelle A contained aqueous solution of Fe(NO₃)₃ and Al(NO₃)₃, and the mixing ratio was adjusted to obtain the different samples, x = 0.06, 0.09, 0.21, 0.30, and 0.40. The sintering temperature was 1050°C for x = 0.06, 0.09, 0.30, and 0.40, and 1025°C for x = 0.21. Only the sample for x = 0 was prepared by an impregnation method using mesoporous silica nanoparticles. The SiO₂ matrices for all samples were etched by NaOH solution. The morphology and size of the obtained samples were examined using transmission electron microscopy (TEM), which showed spherical nanoparticles with an average particle size between 20-50 nm (Figure 4).
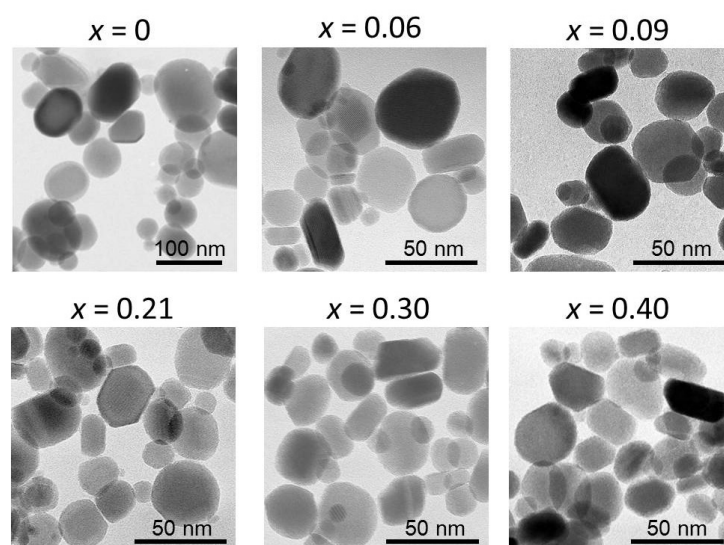

Figure 4. Transmission electron microscopy images of ε-Al$_x$Fe$_{2-x}$O₃ samples. The black bars indicate the scale.

3.2. Al-substitution effect in crystal structure and magnetic properties

X-ray diffraction (XRD) patterns indicated the samples to have the same orthorhombic crystal structure as the original ε-Fe₂O₃. The Rietveld analyses of the XRD patterns showed a constant decrease in the lattice constants with the degree of Al-substitution. The analysis results also indicated that the Al^{3+} ions introduced in the samples have site selectivity in the substitution. For example, in the x = 0.21 sample, the Al^{3+} substitution ratio of each Fe site was 0%, 3%, 8%, and 30% for A, B, C, and D site, respectively. This tendency for the Al^{3+} ion to prefer D site was consistent with all of the Al-substituted samples (Figure 5). This site

selectivity can be understood by the smaller ion radius of Al^{3+} (0.535 Å) compared to Fe^{3+} (0.645 Å) [37]. The Al^{3+} ions prefer to occupy the smaller tetrahedral D site than the octahedral A, B, and C sites.
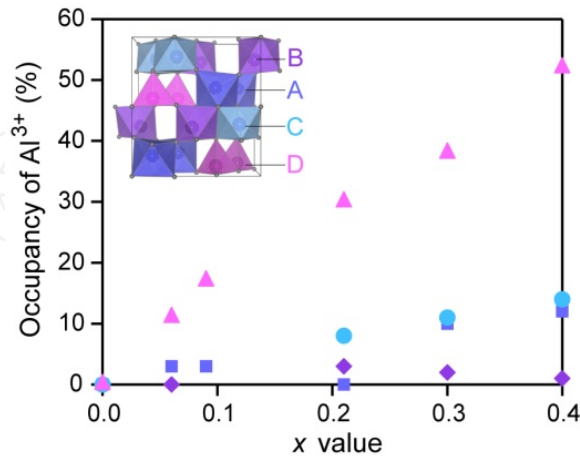

Figure 5. Al^{3+} occupancy ratio for A, B, C, and D site. Square, diamond, circle, and triangle plots represent A, B, C, and D site, respectively. Inset is the crystal structure of ε-Fe_2O_3.

The magnetic properties of the samples are shown in Table 1. The field-cooled magnetization curves under an external magnetic field of 10 Oe showed that the T_C value decreased from 500 K to 448 K with the increase of Al-substitution (Figure 6, upper right). From the magnetization versus external magnetic field measurements, gradual change of the hysteresis loops was also observed. The obtained hysteresis loops of $x = 0$, 0.21, and 0.40 samples are shown in Figure 6. With Al-substitution, the H_c value decreased from 22.5 kOe to 10.2 kOe, and saturation magnetization (M_s) value increased. These changes in the magnetic properties can be explained by the metal replacement of Fe^{3+} magnetic ions ($3d^5$, $S = 5/2$) by non-magnetic Al^{3+} ions ($3d^0$, $S = 0$). As mentioned previously, ε-Fe_2O_3 is a ferrimagnet with positive sublattice magnetizations at B and C sites and negative sublattice magnetizations at A and D sites. With the substitution of D site Fe^{3+} ions with non-magnetic Al^{3+}, the total magnetization increases, leading to the increase of M_s value. In addition, the non-magnetic Al^{3+} ions reduce the superexchange interaction between the magnetic sites, resulting in a decrease of T_C [32]. In this way, the magnetic properties can be widely controlled by Al-substitution.

x	T_C (K)	H_c (kOe)	M_s (emu/g)
0	500	22.5	14.9
0.06	496	19.1	15.1
0.09	490	17.5	14.6
0.21	480	14.9	17.0
0.30	466	13.8	20.3
0.40	448	10.2	19.7

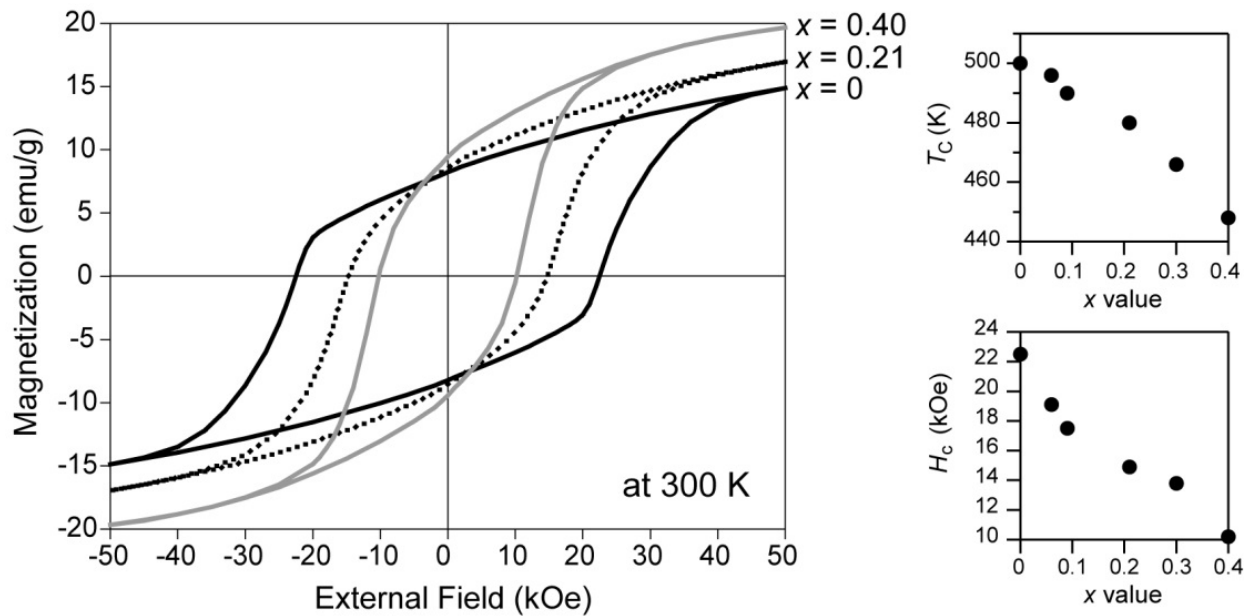**Table 1.** Magnetic properties of ε-$Al_xFe_{2-x}O_3$.

Figure 6. Magnetization versus external magnetic field curve at 300 K for the samples $x = 0$, 0.21, and 0.40 (left), Curie temperature (T_C) versus x value plot (upper right), and coercive field (H_c) versus x value plot (lower right).

3.3. Electromagnetic wave absorption of Al-substituted ε-Fe₂O₃ by zero-field ferromagnetic resonance

Zero-field ferromagnetic resonance is a resonance phenomenon caused by the gyromagnetic effect induced by an electromagnetic wave irradiation under no magnetic field (Figure 7). This phenomenon is observed in ferromagnetic materials with magnetic anisotropy. When the magnetization is tilted away from the easy-axis by the magnetic component of the electromagnetic wave, precession of the magnetization occurs around the easy-axis due to gyromagnetic effect. Resonance is observed when this precession frequency coincides with the electromagnetic wave frequency, resulting in electromagnetic wave absorption at the particular frequency [38]. This resonance frequency (f_r) is proportional to the magnetocrystalline anisotropy (H_a) and can be expressed as

$$f_r = (\nu / 2\pi)H_a, \tag{3}$$

where ν is the gyromagnetic ratio. If the sample is consisted of randomly oriented particles with uniaxial magnetic anisotropy, the H_a value is proportional to H_c. Therefore, electromagnetic wave absorption at high frequencies is expected with insulating materials exhibiting large coercivity, which is the case for ε-Fe₂O₃ based magnets.

With the general electromagnetic wave absorption measurement using free space absorption measurement system, the absorption frequencies of the present ε-Al$_x$Fe$_{2-x}$O₃ samples exceeded the measurement range, where the maximum is 110 GHz. Therefore, the absorption measurements were conducted using terahertz time domain spectroscopy (THz-TDS) at room temperature. The THz-TDS measurement system is shown in Figure 8. A
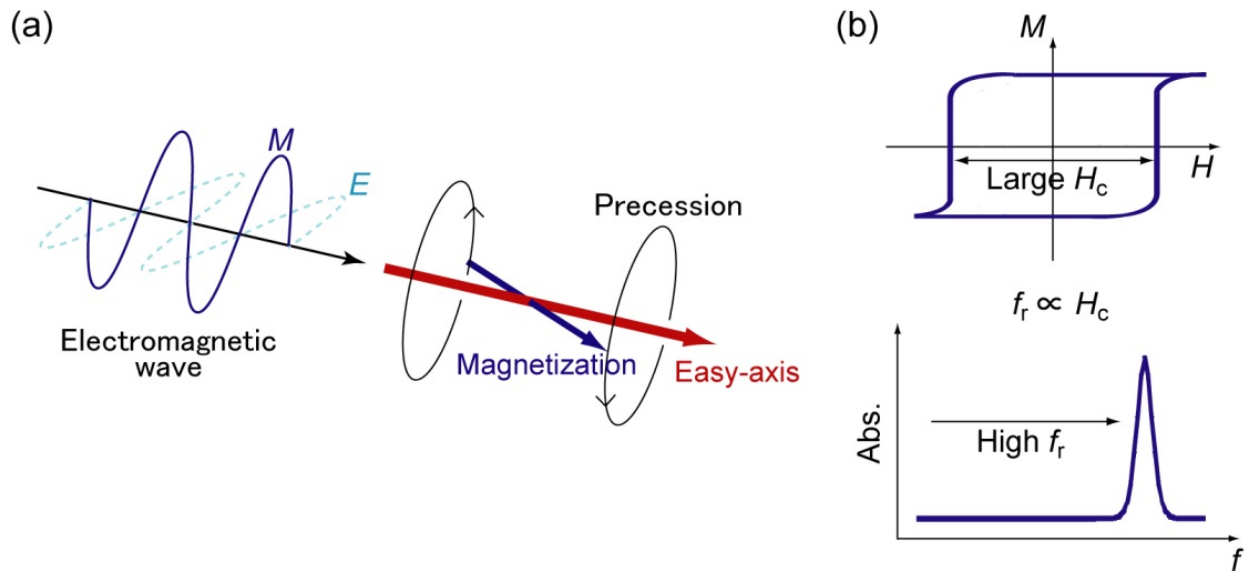
Figure 7. (a) A schematic illustration of zero-field ferromagnetic resonance (natural resonance), resulting in electromagnetic wave absorption due to the precession of magnetization around the easy-axis. The M and E of the electromagnetic wave indicate the magnetic and electric components, respectively. (b) An illustration indicating that larger coercive field (H_c) results in higher resonance frequency (f_r).

mode-locked Ti:sapphire femtosecond pulse laser with a time duration of 20 fs at a repetition rate of 76 MHz was used. The output was divided into a pump and probe beam for the time-domain system. For THz wave emitter and detector, dipole type and bowtie type low-temperature-grown GaAs photoconductive antennas were used, respectively. The sample was set on a sample holder, which was inserted between a set of paraboloidal mirrors concentrating the THz wave at the location of the sample. The temporal waveforms of the electric component of the transmitted THz pulse waves were obtained by changing the delay time between the pump and probe pulses. The temporal waves were Fourier transferred to obtain the frequency dependence, and the absorption spectra were calculated using the following equation:

$$(Absorption) = -10\log|t(\omega)|^2 \ (dB), \tag{4}$$

where $t(\omega)$ is the complex amplitude transmittance. An absorption of 20 dB indicates 99% absorption.

The electromagnetic wave absorption spectra are shown in Figure 9. Absorption peaks were observed at 112 GHz ($x = 0.40$), 125 GHz ($x = 0.30$), 145 GHz ($x = 0.21$), 162 GHz ($x = 0.09$), 172 GHz ($x = 0.06$), and 182 GHz ($x = 0$). The f_r value decreased with Al-substitution, consistent with the behavior of the H_c value (Figure 6, lower right). The observed electromagnetic wave absorption due to zero-field ferromagnetic resonance at exceptional high frequencies was achieved by the large H_a value of this series with large coercivity.
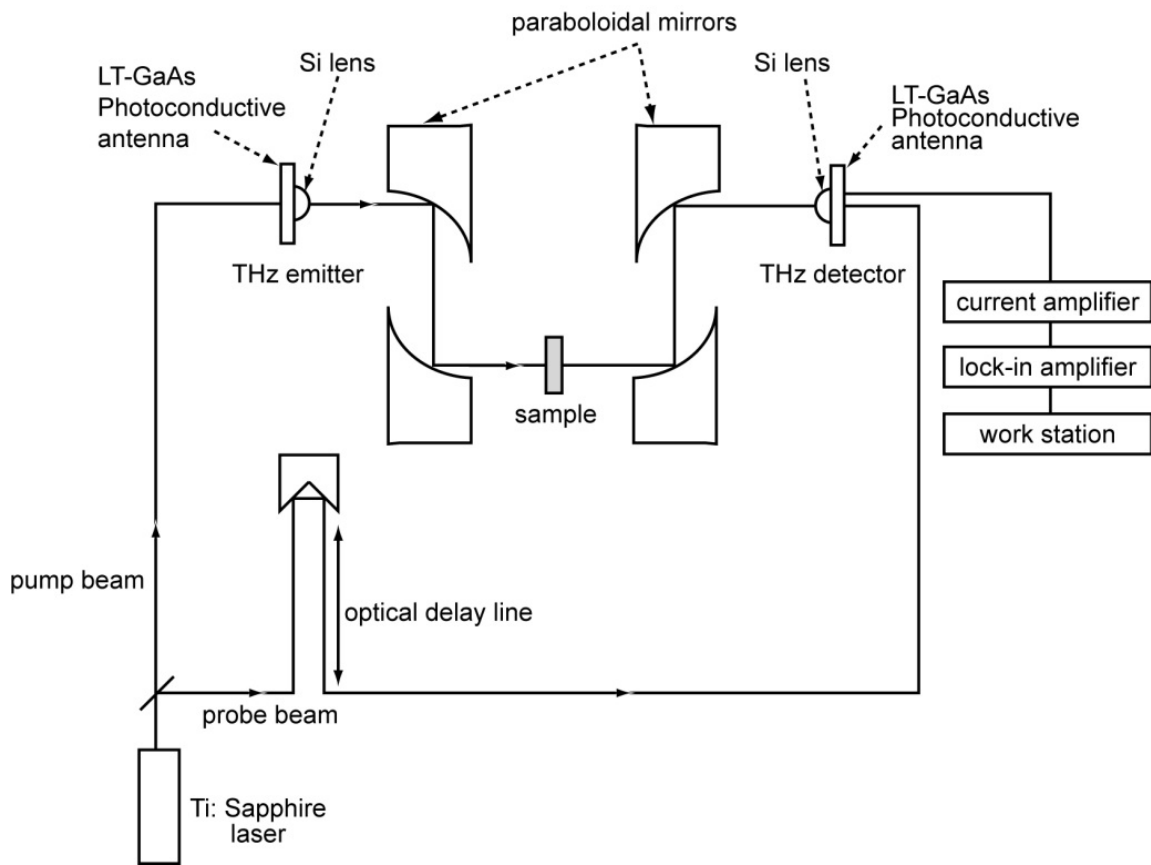
Figure 8. A schematic diagram of the terahertz time domain spectroscopy measurement system.
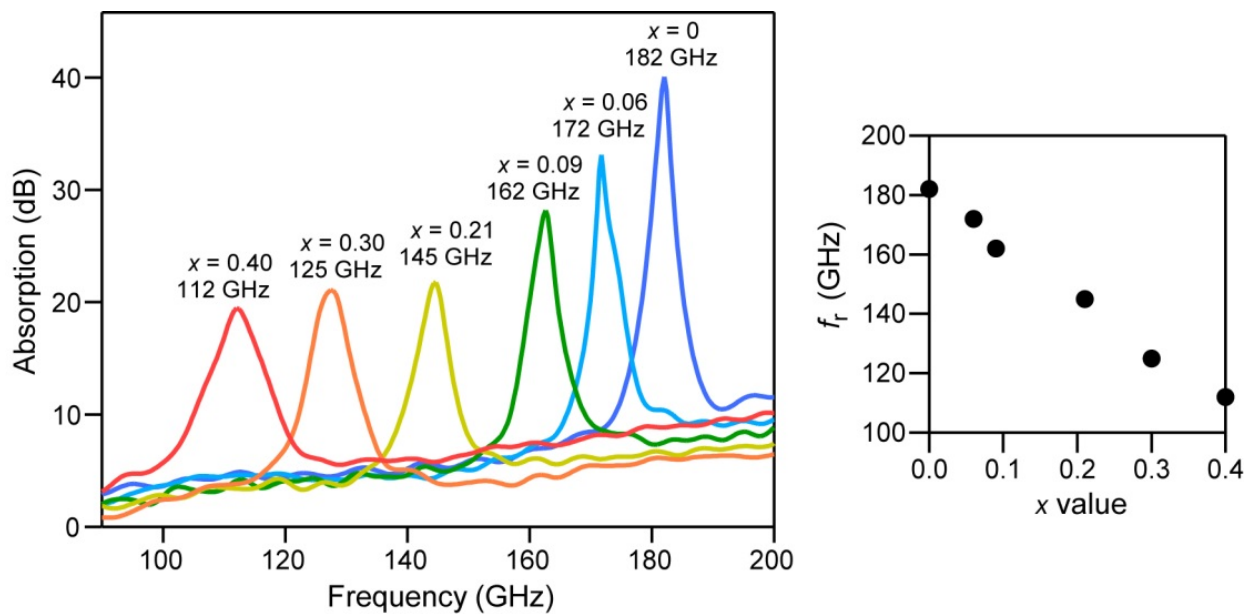

Figure 9. Electromagnetic wave absorption spectra of ε-Al$_x$Fe$_{2-x}$O$_3$ (left). Red, orange, yellow, green, light blue, and blue lines are the absorption spectra for x = 0.40, 0.30, 0.21, 0.09, 0.06, and 0, respectively. Right is the zero-field ferromagnetic resonance frequency (f_r) versus x value plot.

3.4. Temperature dependence of zero-field ferromagnetic resonance in Al-substituted ε-Fe₂O₃

Among the ε-Al$_x$Fe$_{2-x}$O$_3$ samples discussed in the previous section, we focused on the x = 0.06 sample and measured the temperature dependence of zero-field ferromagnetic resonance. The Al^{3+} substitution ratios of each Fe site in ε-Al$_{0.06}$Fe$_{1.94}$O$_3$ are 3%, 0%, 0%, and 11% for A, B, C, and D site, respectively. The magnetic properties of ε-Al$_{0.06}$Fe$_{1.94}$O$_3$ are shown in Figure 10. The field-cooled magnetization curve under 10 Oe external magnetic field showed a T_C value of 496 K and a cusp at 131 K (= T_P). The cusp in the magnetization is due to the spin reorientation phenomenon, which is known to occur in this temperature region [11,12]. The magnetization versus external magnetic field curve exhibited an H_c value of 19.1 kOe at 300 K.
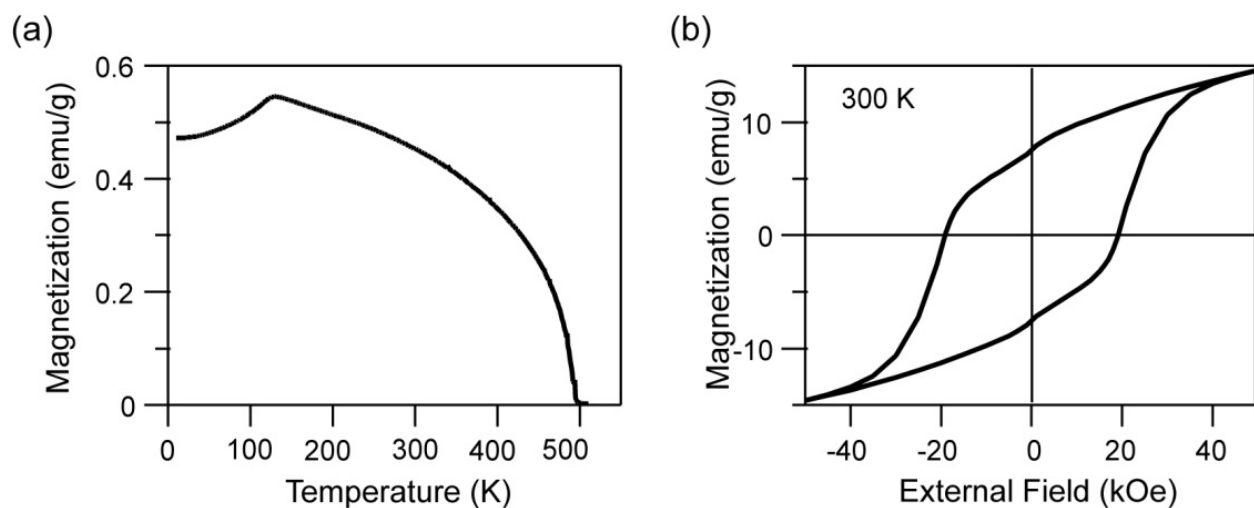

Figure 10. Magnetic properties of ε-Al$_{0.06}$Fe$_{1.94}$O$_3$. (a) Field-cooled magnetization curve under an external magnetic field of 10 Oe. (b) Magnetization versus external magnetic field curve at 300 K.

For the THz-TDS measurement, ε-Al$_{0.06}$Fe$_{1.94}$O$_3$ powder sample was pressed into a pellet-form. The absorption spectra at different temperatures are shown in Figure 11a. These absorption spectra versus frequency were obtained by calibration of the background noise. They were also fitted by Lorentz function. At 301 K, the f_r value was 172 GHz, consistent with the result in the previous section. With the decrease of temperature, the f_r value gradually increased to 186 GHz at 204 K, and turned to an abrupt decrease down to 147 GHz at 77 K. The f_r value continued to decrease with lowering the temperature, and at 21 K, the f_r value was 133 GHz (Figure 11b). Temperature dependence was also observed in the linewidth of the absorption spectra. The full width at half maximum (Δf) value increased from 5 GHz at 301 K to 19 GHz at 77 K with decreasing temperature, and then, decreased to 16 GHz at 21 K (Figure 11c).

Temperature dependencies of magnetic hysteresis loop and ac magnetic susceptibility was studied in order to understand the anomalous temperature dependencies of f_r and Δf. As mentioned in Figure 10a, the field-cooled magnetization curve shows an increase below T_C, but a cusp appears at T_P = 131 K, where the magnetization turns to a decrease. The H_c value

increased from 19.4 kOe at 300 K to 22.6 kOe at 200 K, and then decreased to 4.5 kOe at 70 K with the decrease of temperature. The H_c versus temperature plot indicates a sigmoid decrease in a wide temperature range of 200 – 60 K centered at T_P (i.e., ±70 K from the center temperature, T_P = 131 K) (Figure 12a). In other words, the beginning and ending temperatures of the spin reorientation are about 200 K and 60 K, respectively, with decreasing temperature. The temperature region of the sigmoid decrease of f_r almost corresponds to the temperature range of the spin reorientation. The sigmoid increase of Δf
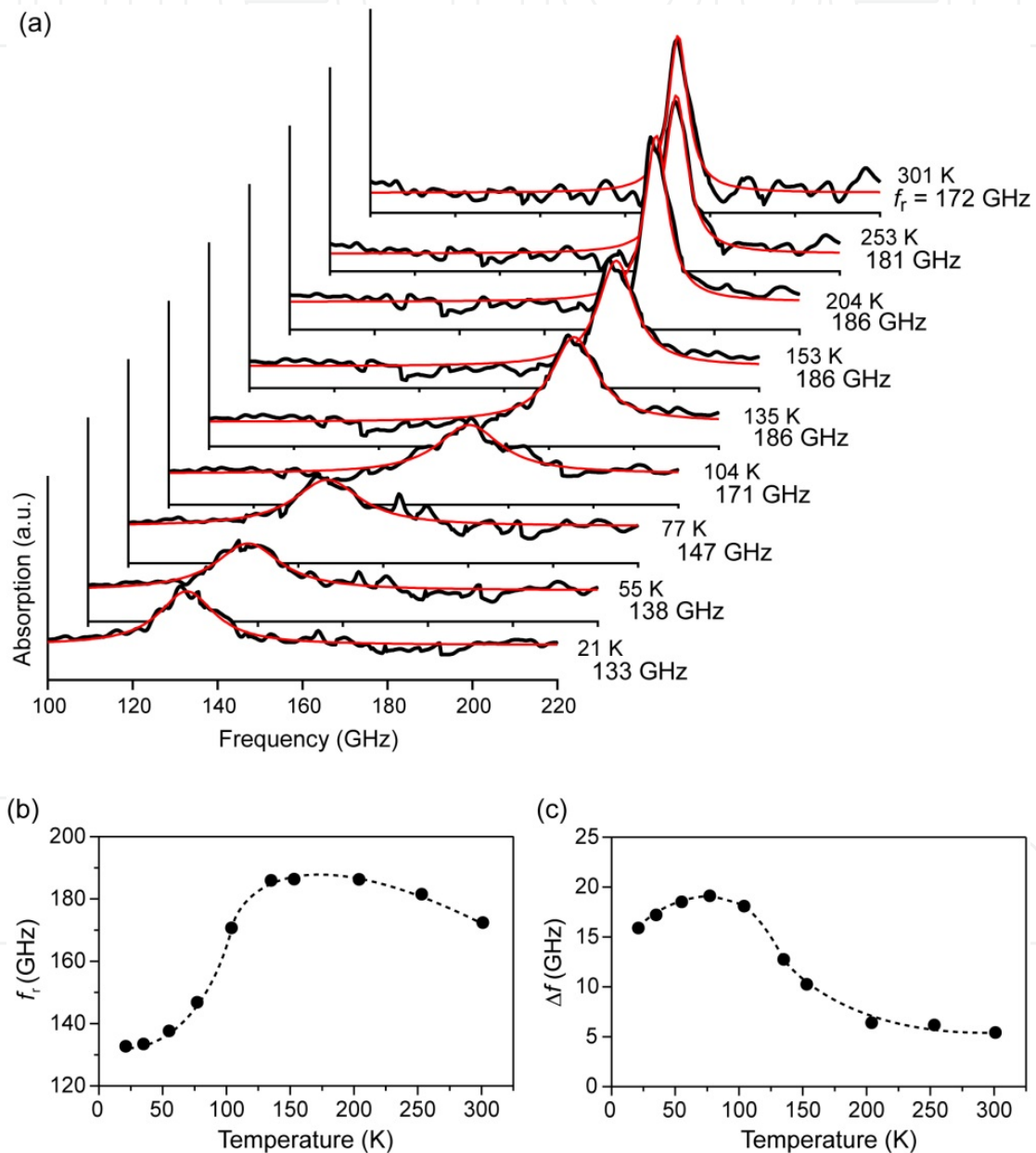
Figure 11. (a) Electromagnetic wave absorption spectra of ε-Al$_{0.06}$Fe$_{1.94}$O$_3$ at different temperatures. Black lines and red lines indicate the observed spectra and fitted Lorentz function. (b) Temperature dependence of zero-field ferromagnetic resonance frequency (f_r). (c) Temperature dependence of full width at half maximum (Δf) of the absorption spectra. Dotted lines are to guide the eye.

was also observed in the spin reorientation temperature region. Figure 12b is the ac magnetic susceptibility versus temperature with frequency of 10 Hz under field amplitude of 1 Oe. As the temperature decreased, the real part of the ac magnetic susceptibility (χ') gradually increased to a maximum value of 3.8×10^{-4} emu/g·Oe at 60 K and then decreased. The imaginary part (χ'') showed similar temperature dependence with a maximum around 70 K. These temperature dependencies of ac magnetic susceptibility correspond to that of Δf [39,40].
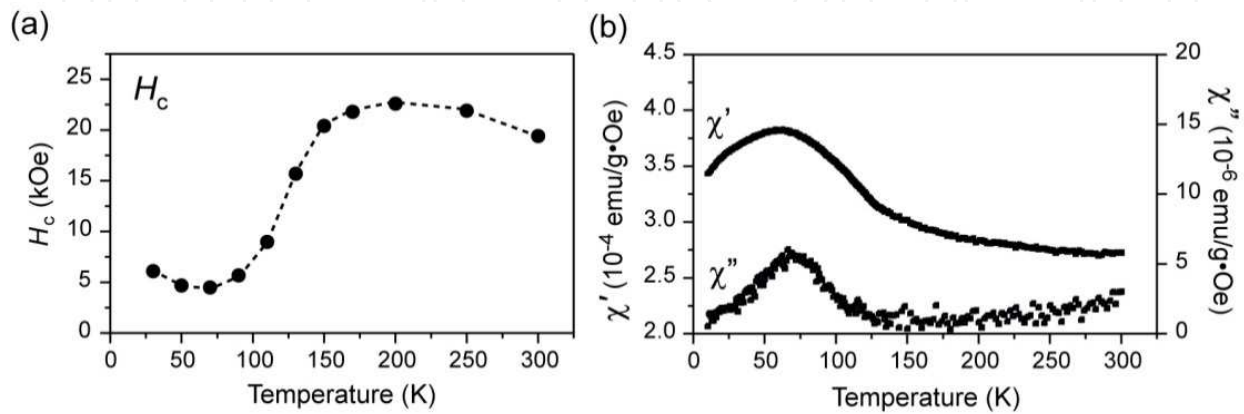
Figure 12. (a) Temperature dependence of coercive field (H_c). Dotted line is to guide the eye. (b) Temperature dependence of ac magnetic susceptibility (real part χ' and imaginary part χ'') measured at 10 Hz and 1 Oe field amplitude.

As mentioned previously, the f_r value is proportional to the H_a value, and in this case with randomly oriented samples, f_r is also related to the H_c value. Therefore, the observed anomalous temperature dependence of f_r in ε-$Al_{0.06}Fe_{1.94}O_3$ was understood by the temperature dependence of H_c. The sigmoid decrease centered at T_P originates from the disappearance of magnetic anisotropy due to the spin reorientation phenomenon [11–13].

4. Conclusion

In this chapter, a rare phase of diiron trioxide, ε-Fe_2O_3, and its Al-substituted series were introduced. The synthesis, crystal structure, and its exceptional physical properties were discussed, especially its huge magnetic anisotropy exhibiting a gigantic coercive field, which enables electromagnetic wave absorption due to zero-field ferromagnetic resonance at high frequencies in the millimeter wave region. Al-substitution effect was observed in the ε-$Al_xFe_{2-x}O_3$ series, widely controlling the magnetic properties and the zero-field ferromagnetic resonance frequency: ε-$Al_xFe_{2-x}O_3$ absorbed millimeter waves from 112–182 GHz at room temperature. Temperature dependence of zero-field ferromagnetic resonance was also investigated for ε-$Al_{0.06}Fe_{1.94}O_3$ sample, and an anomalous behavior was observed due to spin reorientation phenomenon.

Since ε-$Al_xFe_{2-x}O_3$ is composed of very common and low costing elements, it is friendly to the environment and can be economically produced. Its chemical stability is also an

advantage in the viewpoint of industrial applications, such as electromagnetic wave absorbers in the near future, where high-frequency millimeter waves are likely to be used in order to transport heavy data at high speed.

Author details

Marie Yoshikiyo, Asuka Namai and Shin-ichi Ohkoshi
Department of Chemistry, School of Science, The University of Tokyo, Tokyo, Japan

Shin-ichi Ohkoshi
CREST, JST, K's Gobancho, 7 Gobancho, Chiyoda-ku, Tokyo, Japan

Acknowledgement

5. References

[1]   Zhou ZG. Magnetic Ferrite Materials. Beijing: Science Press; 1981.

[2]   Yoshida S, Sato M, Sugawara E, Shimada Y. Permeability and Electromagnetic-Interference Characteristics of Fe-Si-Al Alloy Flakes-Polymer Composite. J. Appl. Phys. 1999;85(8) 4636–4638.

[3]   Naito Y, Suetake K. Application of Ferrite to Electromagnetic Wave Absorber and its Characteristics. IEEE Trans. Microwave Theory Tech. 1971;MT19(1) 65–72.

[4]   Yusoff AN, Abdullah MH, Ahmed SH, Jusoh SF, Mansor AA, Hamid SAA. Electromagnetic and Absorption Properties of Some Microwave Absorbers. J. Appl. Phys. 2002;92 (2) 876–882.

[5]   Adam JD, Davis LE, Dionne GF, Schloemann EF, Stitzer SN. Ferrite Devices and Materials. IEEE Trans. Microwave Theory Tech. 2002;50(3) 721–737.

[6]   Federici J, Moeller L. Review of Terahertz and Subterahertz Wireless Communications. J. Appl. Phys. 2010;107(11) 111101.

[7]   Khatib M. Wireless Communications. Rijeka: Intech; 2011.

[8]   Jin J, Ohkoshi S, Hashimoto K. Giant Coercive Field of Nanometer-Sized Iron Oxide. Adv. Mater. 2004;16(1) 48–51.

[9]   Ohkoshi S, Sakurai S, Jin J, Hashimoto K. The Addition Effects of Alkaline Earth Ions in the Chemical Synthesis of ε-Fe_2O_3 Nanocrystals that Exhibit a Huge Coercive Field. J. Appl. Phys. 2005;97(10) 10K312.

[10] Jin J, Hashimoto K, Ohkoshi S. Formation of Spherical and Rod-Shaped ε-Fe_2O_3 Nanocrystals with a Large Coercive Field. J. Mater. Chem. 2005;15(19) 1067–1071.

[11] Sakurai S, Jin J, Hashimoto K, Ohkoshi S. Reorientation Phenomenon in a Magnetic Phase of ε-Fe_2O_3 Nanocrystal. J. Phys. Soc. Jpn. 2005;74(7) 1946–1949.

[12] Kurmoo M, Rehspringer J, Hutlova A, D'Orleans C, Vilminot S, Estournes C, Niznansky D. Formation of Nanoparticles of ε-Fe_2O_3 from Yttrium Iron Garnet in a Silica Matrix: An Unusually Hard Magnet with a Morin-Like Transition below 150 K. Chem. Mater. 2005;17(5) 1106–1114.

[13] Gich M, Frontera C, Roig A, Taboada E, Molins E, Rechenberg HR, Ardisson JD, Macedo WAA, Ritter C, Hardy V, Sort J, Skumryev V, Nogués J. High- and Low-Temperature Crystal and Magnetic Structures of ε-Fe_2O_3 and their Correlation to its Magnetic Properties. Chem. Mater. 2006;18(16) 2889–2897.

[14] Tucek J, Ohkoshi S, Zboril R. Room-Temperature Ground Magnetic State of ε-Fe_2O_3: In-Field Mössbauer Spectroscorpy Evidence for Collinear Ferrimagnet. Appl. Phys. Lett. 2011;99(25) 253108.

[15] Sakurai S, Shimoyama J, Hashimoto K, Ohkoshi S. Large Coercive Field in Magnetic-Field Oriented ε-Fe_2O_3 Nanorods. Chem. Phys. Lett. 2008;458(4–6) 333–336.

[16] Sakurai S, Tomita K, Hashimoto K, Yashiro H, Ohkoshi S. Preparation of the Nanowire Form of ε-Fe_2O_3 Single Crystal and a Study of the Formation Process. J. Phys. Chem. C 2008;112(34) 13095–13098.

[17] Sakurai S, Namai A, Hashimoto K, Ohkoshi S. First Observation of Phase Transformation of All Four Fe_2O_3 Phases ($\gamma \rightarrow \varepsilon \rightarrow \beta \rightarrow \alpha$-Phase). J. Am. Chem. Soc. 2009;131(51) 18299–18303.

[18] Tucek J, Zboril R, Namai A, Ohkoshi S. ε-Fe_2O_3: An Advanced Nanomaterial Exhibiting Giant Coercive Field, Millimeter-Wave Ferromagnetic Resonance, and Magnetoelectric Coupling. Chem. Mater. 2010;22(24) 6483–6505.

[19] Sakurai S, Kuroki S, Tokoro H, Hashimoto K, Ohkoshi S. Synthesis, Crystal Structure, and Magnetic Properties of ε-$In_xFe_{2-x}O_3$ Nanorod-Shaped Magnets. Adv. Funct. Mater. 2007;17(14) 2278–2282.

[20] Namai A, Sakurai S, Ohkoshi S. Synthesis, Crystal Structure, and Magnetic Properties of ε-$Ga^{III}_xFe^{III}_{2-x}O_3$ Nanorods. J. Appl. Phys. 2009;105(7) 07B516.

[21] Yamada K, Tokoro H, Yoshikiyo M, Yorinaga T, Namai A, Ohkoshi S. Phase Transition of ε-In$_x$Fe$_{2-x}$O$_3$ Nanomagnets with a Large Thermal Hysteresis Loop. J. Appl. Phys. 2012;111(7) 07B506.

[22] Ohkoshi S, Kuroki S, Sakurai S, Matsumoto K, Sato K, Sasaki S. A Millimeter-Wave Absorber Based on Gallium-Substituted ε-Iron Oxide Nanomagnets. Angew. Chem. Int. Ed. 2007;46(44) 8392–8395.

[23] Namai A, Sakurai S, Nakajima M, Suemoto T, Matsumoto K, Goto M, Sasaki S, Ohkoshi S. Synthesis of an Electromagnetic Wave Absorber for High-Speed Wireless Communication. J. Am. Chem. Soc. 2009;131(3) 1170–1173.

[24] Namai A, Kurahashi S, Hachiya H, Tomita K, Sakurai S, Matsumoto K, Goto T, Ohkoshi S. High Magnetic Permeability of ε-Ga$_x$Fe$_{2-x}$O$_3$ Magnets in the Millimeter Wave Region. J. Appl. Phys. 2010;107(9) 09A955.

[25] Nakajima M, Namai A, Ohkoshi S, Suemoto T. Ultrafast Time Domain Demonstration of Bulk Magnetization Precession at Zero Magnetic Field Ferromagnetic Resonanace Induced by Terahertz Magntic Field. Opt. Express 2010;18(17) 18260–18268.

[26] Afsar MN, Korolev KA, Namai A, Ohkoshi S. Measurements of Complex Magnetic Permeability of Nano-Size ε-Al$_x$Fe$_{2-x}$O$_3$ Powder Materials at Microwave and Millimeter Wavelengths. IEEE Trans. Magn. 2012;48(11) 2769–2742.

[27] Namai A, Kurahashi S, Goto T, Ohkoshi S. Theoretical Design of a High-Frequency Millimeter Wave Absorbing Sheet Composed of Gallium Substituted ε-Fe$_2$O$_3$ Nanomagnet. IEEE Trans. Magn. 2012;48(11) 4386–4389.

[28] Yoshikiyo M, Namai A, Nakajima M, Suemoto T, Ohkoshi S. Anomalous Behavior of High-Frequency Zero-Field Ferromagnetic Resonance in Aluminum-Substituted ε-Fe$_2$O$_3$. J. Appl. Phys. 2012;111(7) 07A726.

[29] Namai A, Yoshikiyo M, Yamada K, Sakurai S, Goto T, Yoshida T, Miyazaki T, Nakajima M, Suemoto T, Tokoro H, Ohkoshi S. Hard Magnetic Ferrite with a Gigantic Coercivity and High Frequency Millimetre Wave Rotation. Nat. Commun. 2012;3 1035.

[30] Möller K, Kobler J, Bein T. Collidal Suspensions of Nanometer-Sized Mesoporous Silica. Adv. Funct. Mater. 2007;17(4) 605–612.

[31] Haneda K, Miyakawa C, Kojima H. Preparation of High-Coercivity BaFe$_{12}$O$_{19}$. J. Am. Ceram. Soc. 1974;57(8) 354–357.

[32] Ohkoshi S, Namai A, Sakurai S. The Origin of Ferromagnetism in ε-Fe$_2$O$_3$ and ε-Ga$_x$Fe$_{2-x}$O$_3$ Nanomagnets. J. Phys. Chem. C 2009;113(26) 11235–11238.

[33] Yoshikiyo M, Yamada K, Namai A, Ohkoshi S. Study of the Electronic Structure and Magnetic Properties of ε-Fe$_2$O$_3$ by First-Principles Calculation and Molecular Orbital Calculations. J. Phys. Chem. C 2012;116(15) 8688–8691.

[34] McHale JM, Auroux A, Perrotta AJ, Navrotsky A. Surface Energies and Thermodynamic Phase Stability in Nanocrystalline Aluminas. Science 1997;277(5327) 788–791.

[35] Wen HL, Chen YY, Yen FS, Huang CH. Size Characterization of θ- and α-Al$_2$O$_3$ Crystallites During Phase Transformation. Nanostruct. Mater. 1999;11(1) 89–101.

[36] Ohkoshi S, Tsunobuchi Y, Matsuda T, Hashimoto K, Namai A, Hakoe F, Tokoro H. Synthesis of a Metal Oxide with a Room-Temperature Photoreversible Phase Transition. Nat. Chem. 2010;2(7) 539–545.

[37] Shannon RD. Revised Effective Ionic Radii and Systematic Studies of Interatomic Distances in Halides and Chalcogenides. Acta Cryst. 1976;A32(Sep1) 751–767.

[38] Chikazumi S. Physics of Ferromagnetism. New York: Oxford University Press; 1997.

[39] Algarabel PA, Moral A, Ibarra MR, Arnaudas JI. Spin Reorientation in $ReCo_5$ Compounds: A.C. Susceptibility and Thermal Expansion. J. Phys. Chem. Solids 1988;49(2) 213–222.

[40] Malik SK, Adroja DT, Ma BM, Boltich EB, Sohn JG, Sankar SG, Wallace WE. Spin Reorientation Phenomenon in $Nd_{0.5}Er_{1.5}Fe_{14-x}M_xB$ (M = Al and Co), as Determined by AC Susceptibility Measurements. J. Appl. Phys. 1990;67(9) 4589–4591.